9.2 EFFECTS OF IMPINGING LOCATION AND ANGLE OF AN IDEALIZED TROPICAL CYCLONE ON A LONG MOUNTAIN RANGE

Liping Liu[1]*, Yuh-Lang Lin[2,3], and Shu-Hua Chen[4]
Department of Mathematics[1]
Department of Physics[2]
Department of Energy and Environmental Systems [3]
North Carolina A&T State University, Greensboro, NC
Department of Land, Air and Water Resources[4]
University of California, Davis, CA

1. INTRODUCTION

Hurricanes may induce extremely heavy rainfall leading to flash flooding when they pass over a mesoscale mountain range. The locations of those heavy rainfall areas are strongly dependent on the track which tends to be deflected by orography. Therefore, it is important to study the orographic effects on track deflection. In addition it is found that the track deflection of tropical cyclones (TCs) over a mesoscale mountain range is controlled by some dominant non-dimensional parameters, such as basic-flow Froude number, vortex Froude number, mountain slopeness, etc. (e.g., Lin et al. 2005; see Lin 2007 for a brief review). In addition to those control parameters, the impinging location and angle are also found to play important roles on the track deflection of a TC passing over a mesoscale mountain (Lin and Savage 2011)

In this study, we are particularly interested in the effects of impinging location and angle on track deflection when a hurricane passes over the Southern-Central Appalachians (SCA). The track deflection for hurricanes passing over SCA has been categorized into 4 types (Harville 2009, denoted as H09 hereafter): (A) hurricanes coming from the east, (B) hurricanes tracking along the mountain at the eastern side, (C) Same as (B) except at the western side, and (D) hurricanes coming from the west (Fig. 1).

In this study, we extend Lin and Savage's (2011) study to include the initial bogus vortex, the PBL and moisture effects, and the idealized SCA mountains by using a state-of-art numerical weather prediction model, Weather Research and Forecasting (WRF) model. The impinging directions and angles of numerical experiments designed to test various environmental and numerical effects on the track deflection are sketched in Figure 2. Their associated flow and orographic parameters are summarized in Table 1. Types A1-A3 are similar to Track A of H09 except impinging on the northern, central, and southern part of the SC Appalachians, respectively. Types AB1-AB3 are similar to A1-A3, respectively, but from south-southeast. Types D1 and D2 are similar to Track D of H09 except the former crosses over the SC Appalachians, while the latter skirts around the southern tip of the mountains.

* *Corresponding author address*: Dr. Liping Liu, Dept. of Mathematics, North Carolina A&T State Univ., 1601 E. Market St., Greensboro, NC 27411.
E-mail: lliu@ncat.edu

2. THE NUMERICAL MODEL and EXPERIMENTAL DESIGN

The model used for this study is the Advanced Research WRF (ARW) model version 3.4.1 (Skamarock et al. 2008). The ARW model is a three-dimensional, fully compressible, nonhydrostatic model using terrain-following vertical coordinates. The governing equations for ARW are written in flux-form with conserved mass and dry entropy. In this study, the Runge-Kutta third-order time difference scheme is employed, and the fifth- and third-order advection schemes are used for the horizontal and vertical directions, respectively.

For the experiments, we utilize a single domain as illustrated in Figure 3. For the domain, 15 km horizontal resolution with 433 X 433 horizontal grid intervals is used. In the vertical direction, the grids are stretched from the surface to the model top (20 km) with a total of 28 levels. A 5-km deep sponge layer was added to the upper part of the physical domain. A periodic lateral boundary condition is applied at the boundaries of the domain. The domain is integrated for 14 days and initialized by the bogus vortex (Nolan 2011; Nolan et al. 2013).

The following model physics parameterization or representation schemes are chosen for all simulations conducted in this study:

- Kain-Fritsch cumulus parameterization scheme
- Lin et al. or Ferrier microphysics parameterization scheme
- YSU PBL parameterization scheme
- Monin-Obukov surface layer scheme
- Unified NOAH land-surface processes scheme
- Second-order diffusion term on coordinate surfaces for turbulence and mixing processes
- Horizontal Smagorinsky first-order closure for eddy coefficient option.
- No longwave radiation parameterization scheme
- No shortwave radiation parameterization scheme

Details of these schemes and their relevant references can be found in the ARW user manual (Skamarock et al. 2008).

Figure 3 shows the schematics of the mountain, the TC vortex and the basic wind. The idealized mountain is about 1400km long and 200km wide, the mountain height is 1km, which mimics the SCA. The maximum

tangential wind of the TC vortex is about 60 m/s after it is fully developed and the basic wind is 5 m/s. From these numbers, we can roughly estimate out the Froude numbers. The basic flow Froude number is roughly 0.5, which is low, therefore the orographic blocking on the basic flow is strong. On the other hand, the vortex Froude number is roughly 6, which is high, therefore the orographic blocking on the TC vortex is weak. The location of the mountain is 2600km away from the east boundary in *x*-direction and central for the y-direction. The initial bogus vortex is with V_{max} = 20.8 m/s. The location of the initial vortex is 1100km away from the eastern boundary in the x-direction and central in the y-direction. The other configuration is: Δt = 45 s; $\Delta x = \Delta y = 15$ km; (x,y) = (6480, 6480 km); Total time = 12 d. Equation (1) is the formula for the mountain geometry, for the north-south oriented mountain. The x-direction is bell-shaped, and the y-direction is also bell-shaped near the northern/southern tip.

$$h(x,y) = \begin{cases} \dfrac{h_0}{\left(1+\frac{(x-x_0)^2}{a^2}\right)^{3/2}}, & |y-y_0| \le b \\ \dfrac{h_0}{\left(1+\frac{(x-x_0)^2}{a^2}+\frac{(y-y_0)^2}{a^2}\right)^{3/2}}, & |y-y_0| > b \end{cases} \quad (1)$$

Our simulations are based on the more detailed categorization of hurricane track types in Figure 2. The relevant flow and orographic parameters are summarized in Table 1. We choose A2 as our control case to study, when the hurricane impinges on the mountain at the center of the east side.

3. THE MECHANISM OF TRACK DEFLECTION

The 240 h accumulated rainfall (shaded in color) for the control case is shown in Figure 4, together with the wind vectors and vorticity (contoured) at 850mb. The TC track coincides with the accumulated rainfall. Notice that the track is deflected to the south upstream and to the north downstream back to the original direction. The continuous track is related to the weak orographic blocking on the TC vortex. This track deflection may be explained by the conceptual model in Figure 5.

Figure 5a shows the orographic effects on the basic flow, which steers the TC vortex. Briefly speaking, a high pressure is developed by the adiabatic cooling associated with a uniform airflow passing over the mountain, which forces the TC vortex to go over the mountain anticyclonically. Figure 5b shows the orographic effects on the outer circulation of the TC. Upstream (East) of the mountain range, the air-column stretching (shrinking) over the downslope (upslope) to the south (north) associated with the outer circulation of the cyclone vortex will steer the cyclone toward the south upstream; by the same token, downstream the TC vortex is steered northward back to the original direction. The conceptual model here will be verified by the numerical experiments as shown in Figure 6.

The TC has a tendency to move toward the area where the rate of change of relative vorticity (ζ_t) is positive. Figure 6 shows the local rate of change of ζ over a time period (Δt) of 240 h for various times: a) upstream, b) right before the mountain, c) just pass over the mountain, and d) downstream away from the mountain. In panels a) and b), upstream before the mountain, the maximum ζ_t is located to the southwest of the TC, which makes the TC moving southwestward. In panels c) and d), downstream, the maximum of $\partial\zeta/\partial t$ is located to the northwest of the TC, which makes the TC moving northward back to its original direction.

Next, we try to find what contributes to the ζ_t (also called relative vorticity tendency). A vorticity budget analysis has been conducted for this case. The individual terms of the vorticity equation (Eq. (2)) are plotted at the four times. The main contribution is coming from the horizontal advection, the relative vorticity stretching, and the tilting. We found that the vertical advection and planetary vorticity stretching are less significant.

$$\frac{\partial\zeta}{\partial t} = -\mathbf{V}\cdot\boldsymbol{\nabla}\zeta - \omega\frac{\partial\zeta}{\partial p} - \zeta\,\boldsymbol{\nabla}\cdot\mathbf{V} - f\,\boldsymbol{\nabla}\cdot\mathbf{V} + \mathbf{k} \quad (2)$$

At 132 h in Fig. 7, upstream of the mountain, the TC vortex has started to move southwestward. Based on the vorticity budget analysis, it is mainly contributed by the relative vorticity stretching, while compensated by the other terms. At 171 h in Fig. 8, the TC keeps moving southwestward to pass over the mountain, the relative vorticity stretching still dominates the ζ_t. At 183 h in Fig. 9, when the TC passes over the mountain, the maximum relative vorticity tendency is shifted to the northwest, which makes the TC moving northwestward back to its original track. Again, the major contribution to the relative vorticity tendency is still from the relative vorticity stretching. At 204 h in Fig. 10, downstream and away from the mountain, the relative vorticity tendency is dominated by the horizontal advection.

4. EFFECTS OF IMPINGING LOCATIONS AND ANGLES

In this section, we present some details and results about the effects of impinging locations and angles by performing the vorticity budget analysis for various cases. Figure 11 shows the simulated tracks A1, A2, and A3. Track A2 has been discussed and analyzed in the previous section. Notice that track A3 has less deflection southward when it passes over the mountain and its vicinity. This is due to less orographic blocking near the southern tip. Track A1 has less deflection southward too, however, it is due to the stronger vorticity advection around the northern tip.

In Figure 12, for track A1, the maximum ζ_t is located at the west, rather than to the southwest as in the control case A2. This is mainly due to the strong horizontal advection toward northwest. The relative vorticity stretching is more circular. This makes the TC track more straight, compared to the control case A2.

In Figure 13, for track A3, the maximum ζ_t is located to the southwest. So the TC is moving southwestward. After passing over the mountain, the

track is curved northwestward back to its original track. Note that here the relative vorticity stretching is not as strong as those in case A2.

Figure 14 shows the TC tracks for the AB cases. For tracks AB1, AB2 and AB3, the mechanisms of the track deflection are essentially similar to tracks A1, A2, and A3 as we just discussed.

Figure 15 shows the TC tracks for types B and C. The track deflections of B and C are mainly influenced by the vorticity stretching associated with latent heating/moisture effects. The mechanism of the track deflection may be explained by the vorticity budget analysis in Figs. 16 and 17.

In Fig. 16a, it shows that the TC continuous moving along the mountain. At 204 h, the relative vorticity tendency is still mainly dominated by the relative vorticity stretching, as shown in the middle panel. However, the relative vorticity stretching is mainly contributed by the convection/latent heating, instead of the downslope column stretching. Figure 17 is for the other hours, with the similar mechanism. Moreover, this mechanism applies to track Type C too.

5. CONCLUSION

In conclusion, for track type A2, the track deflection is mainly controlled by the vorticity stretching, i.e. deflected to south upstream and then turns back north downstream. For track type A1, the vorticity advection compensates the vorticity stretching making the track less southward. For track type A3, we have less vorticity stretching near the southern tip. Type AB cases are similar to Types A1-A3. For Type B, the relative vorticity stretching is mainly contributed by the convection/latent heating, instead of the downslope column stretching. For future work, we plan to do PV (potential vorticity) budget analysis, to find the sources or sinks of potential vorticity.

ACKNOWLEDGEMENTS: This research was supported by the National Science Foundation Awards AGS-1265783 and OCI-1126543.

6. REFERENCES

Harville, S. L., 2009 (H09): Effects of Appalachian topography on precipitation from landfalling hurricanes. MS thesis, North Carolina State University, 320pp. [Available from http://repository.lib.ncsu.edu/ir/handle/1840.16/2849]

Lin, Y.-L., 2007: *Mesoscale Dynamics*. Cambridge Univ. Press, 630pp. Lin, Y.-L., and L. C. Savage III, 2011: Effects of landfall location and the approach angle of a cyclone vortex encountering a mesoscale mountain range. *J. Atmos. Sci.*, **68**, 2095-2106**.**

Lin, Y.-L., S.-Y. Chen, C. M. Hill, and C.-Y. Huang, 2005: Control parameters for tropical cyclones passing over mesoscale mountains, *J. Atmos. Sci.*, **62**, 1849-1866.

Nolan, D. S., 2011: Evaluating environmental favorableness for tropical cyclone development with the method of point downscaling. *J. Adv. Model. Earth Syst.*, 3, Art. M08001, 28

Nolan, D. S., Robert Atlas, Kieran T. B., and Lisa R. B., 2013: Development and validation of a hurricane nature run using the Joint OSSE Nature Run and the WRF model. *J. Adv. Earth. Model. Syst., 5* , 1-24.

Skamarock, W. C., J. B. Klemp, J. Dudhia, D. O. Gill, D. M. Barker, M. G. Duda, X.-Y. Huang, W. Wang, and J.G. Powers, 2008: A description of the advanced research WRF version 3. NCAR technical note, 113 pp. (also see http://www.mmm.ucar.edu/wrf/users/docs/arw_v3.pdf)

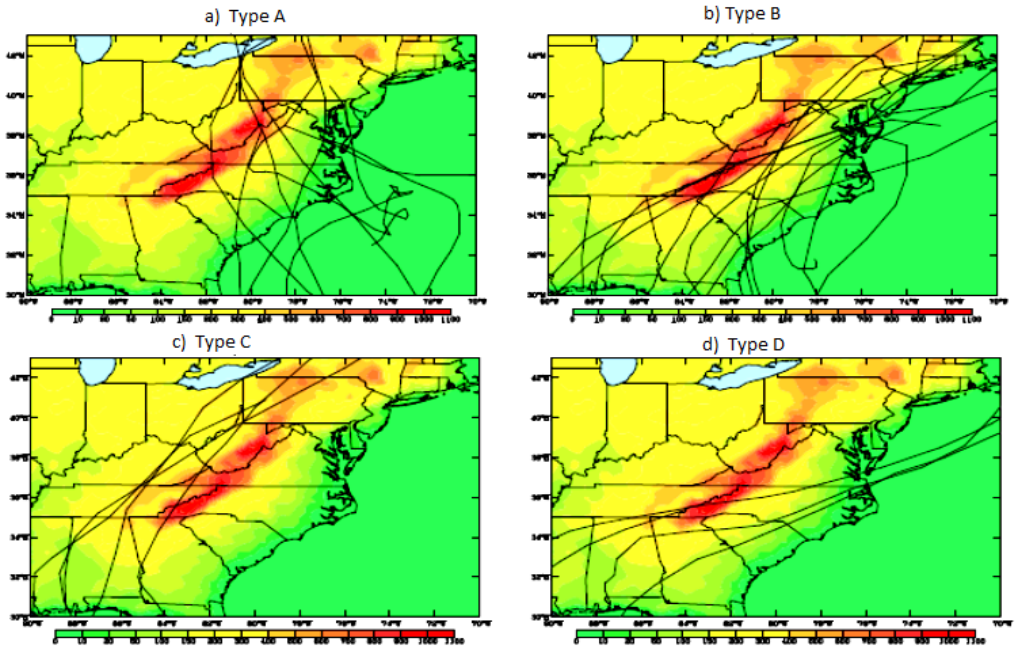

Figure 1: Classification of track types for hurricanes passing over SCA mountains (Harville 2009).

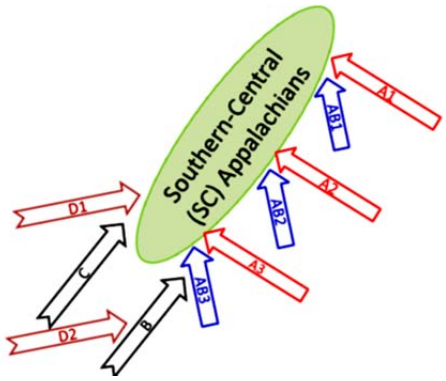

Figure 2: Detailed classification of tropical cyclone (TC) track types over SCA Mountains.

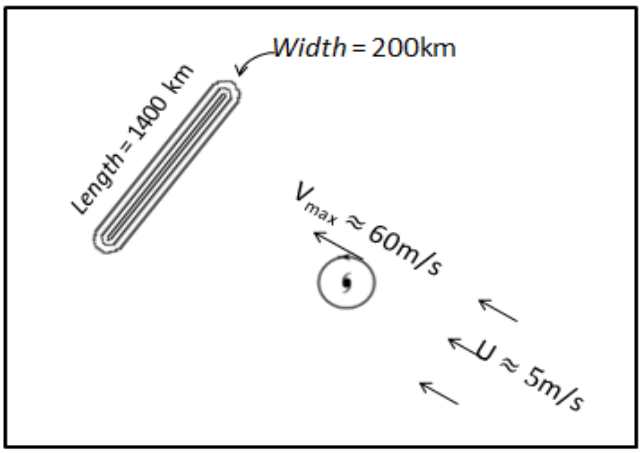

Figure 3: Schematics of the Mountain, the TC vortex and the basic wind.

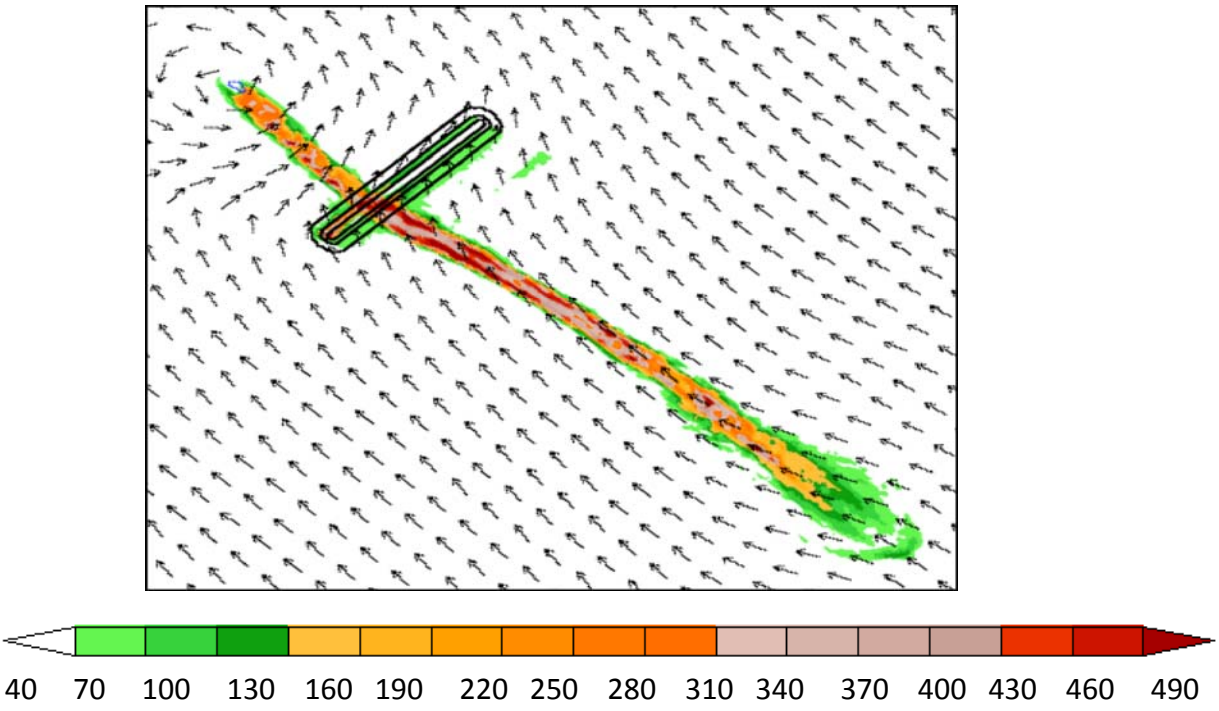

Figure 4: Accumulated rainfall in color shade, 850mb wind vector and vorticity in blue contour.

Table 1. Names, impinging directions, locations, and angles of simulated Cases

Case	Impinging direction (from) & location		Impinge angle (between impinging and mountain directions)
A2 (CNTL)	Easterly	On Center	90^o
A1		On North	
A3		On South	
AB1	South-easterly	On South	45^o
AB2		On Center	
AB3		On North	
B	Southerly along	East Side	0^o
C		West Side	
D1	South-westerly	On South	45^o
D2		Off South	

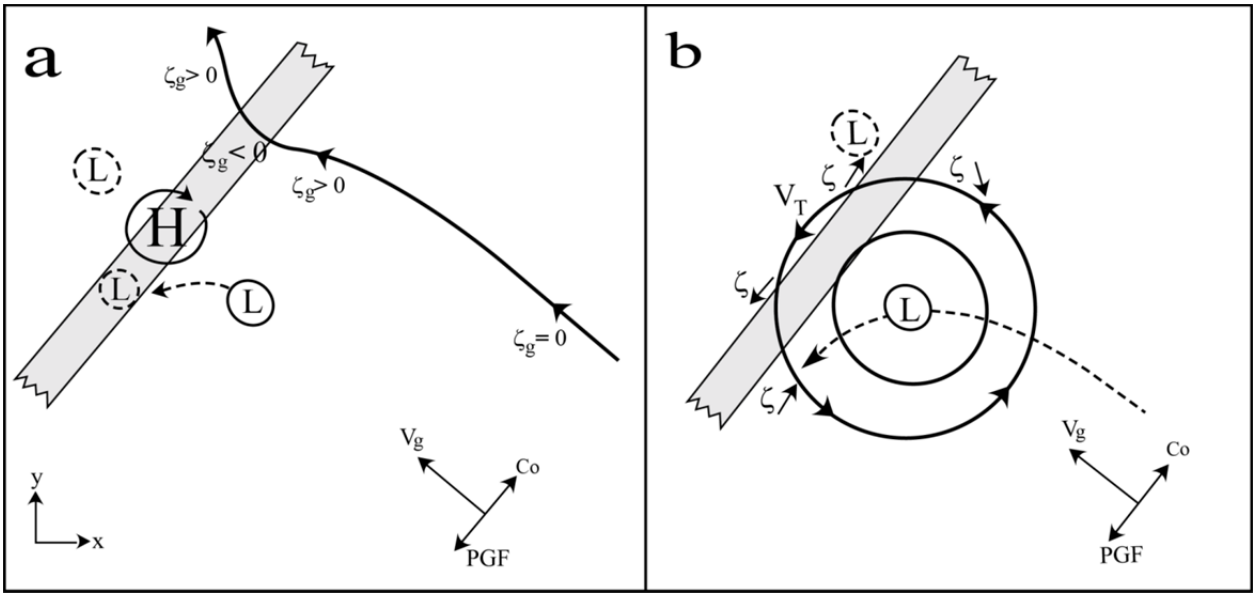

Figure 5: The conceptual model for the track deflection (adopted from Lin 2007): a) Orographic effects on steering flow; b) orographic effects on outer circulation.

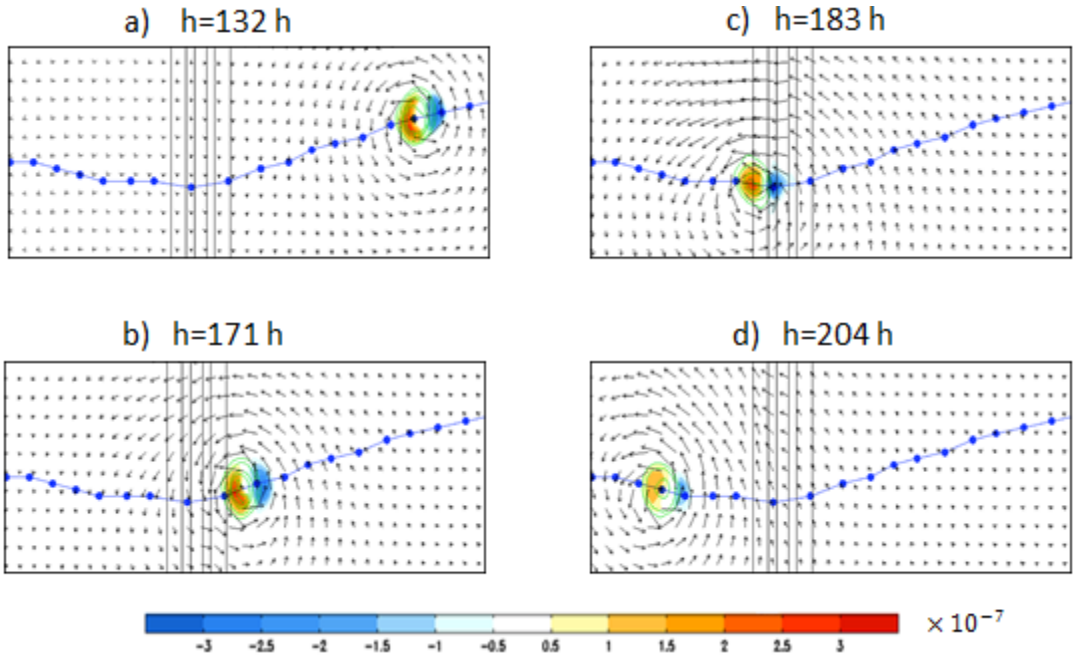

Figure 6: The rate of change of zeta for the control case. A) 132 h before and away from the mountain; b) 171 h right before the TC impinges the mountain; c) 183 h right after the TC passes over the mountain; d) 204 h after and away from the mountain.

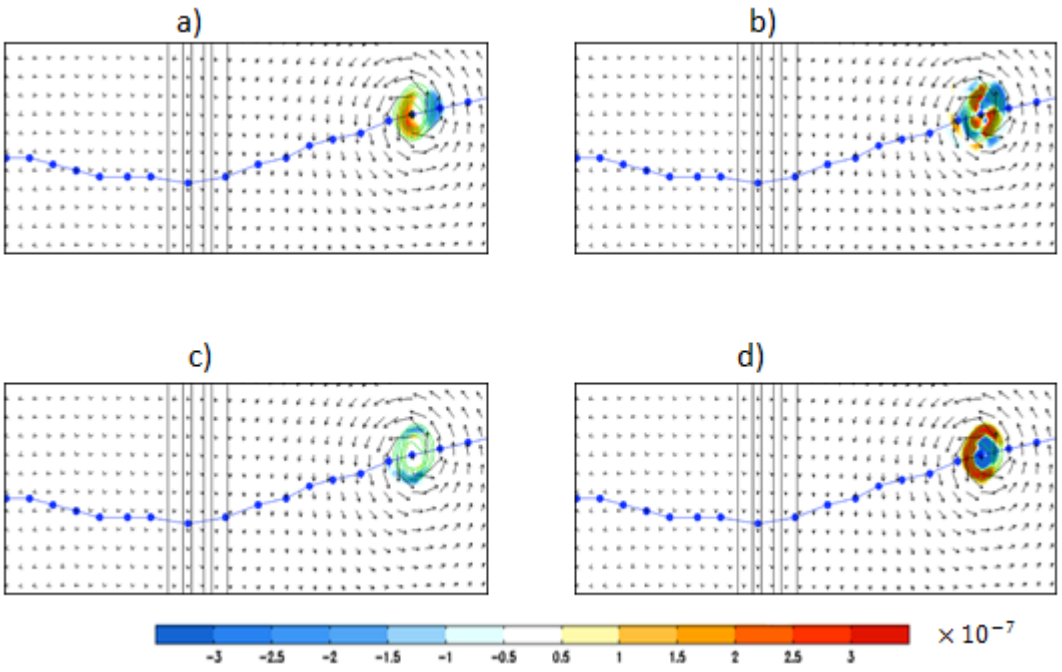

Figure 7: Vorticity budget analysis for the control case at 132 h: a) the local rate of change of ζ (ζ_t); b) the horizontal advection (?); c) the vorticity tilting; d) the relative vorticity stretching.

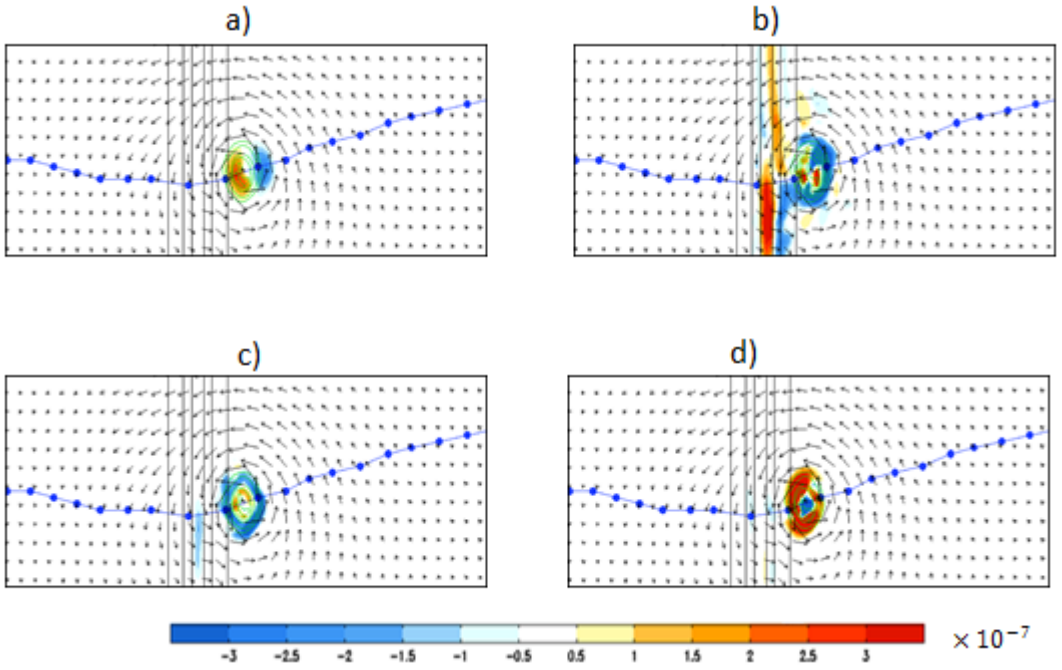

Figure 8: Same as Figure 7 except at 171 h.

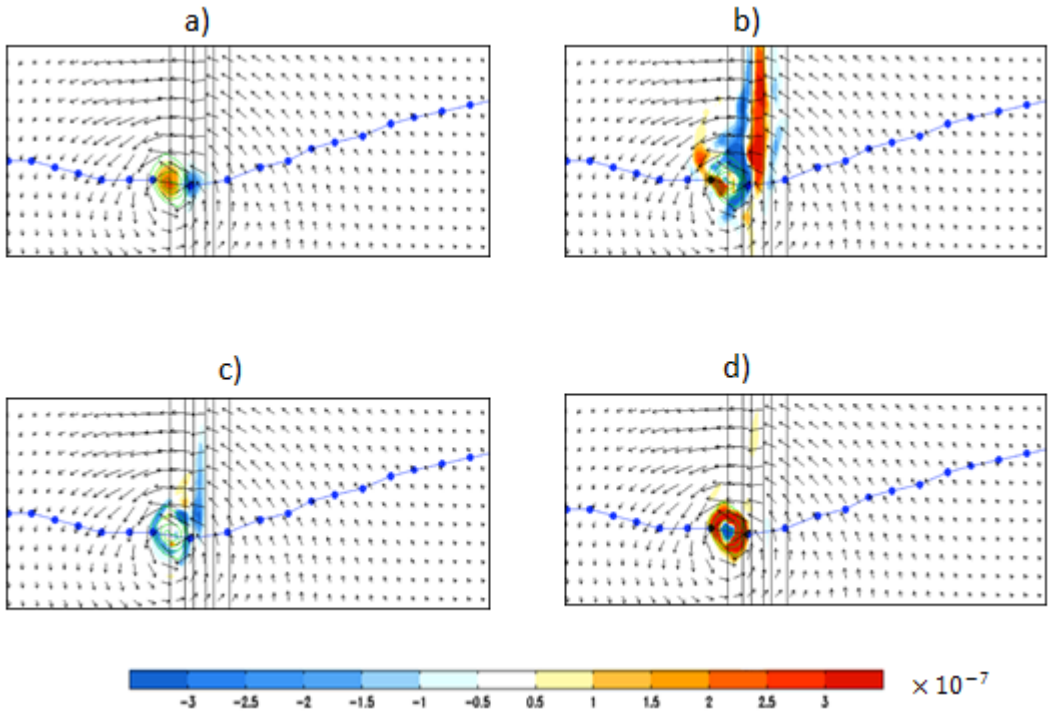

Figure 9: Same as Figure 7 except at 183 h.

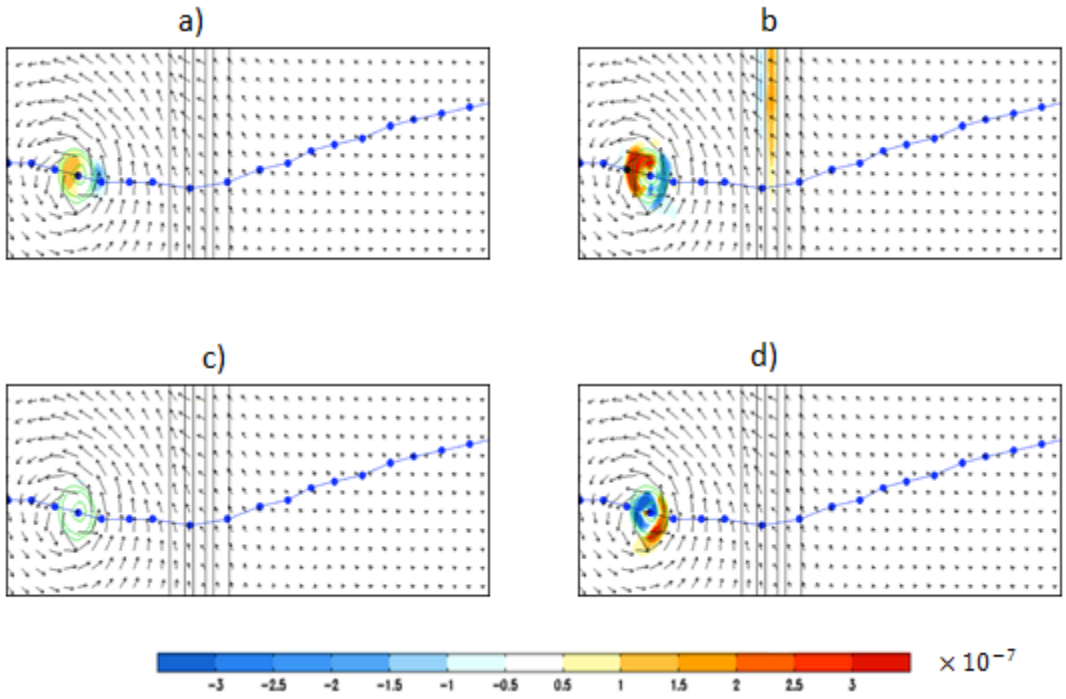

Figure 10: Same as Figure 7 except at 204 h.

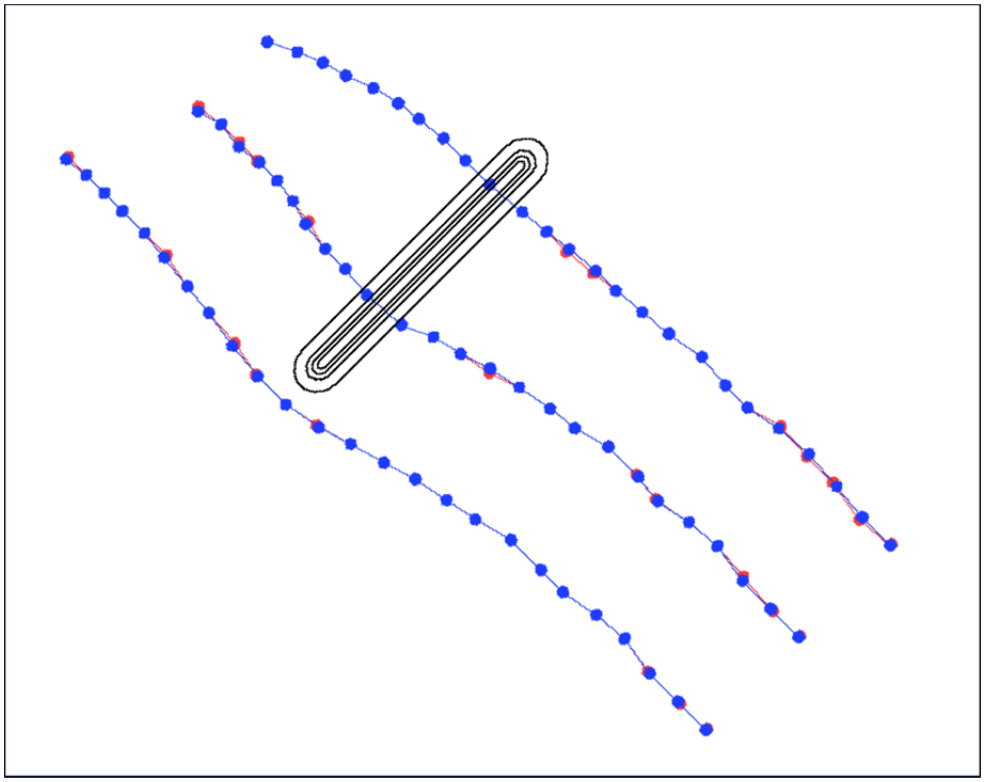

Figure 11: The TC tracks for cases A1, A2 and A3.

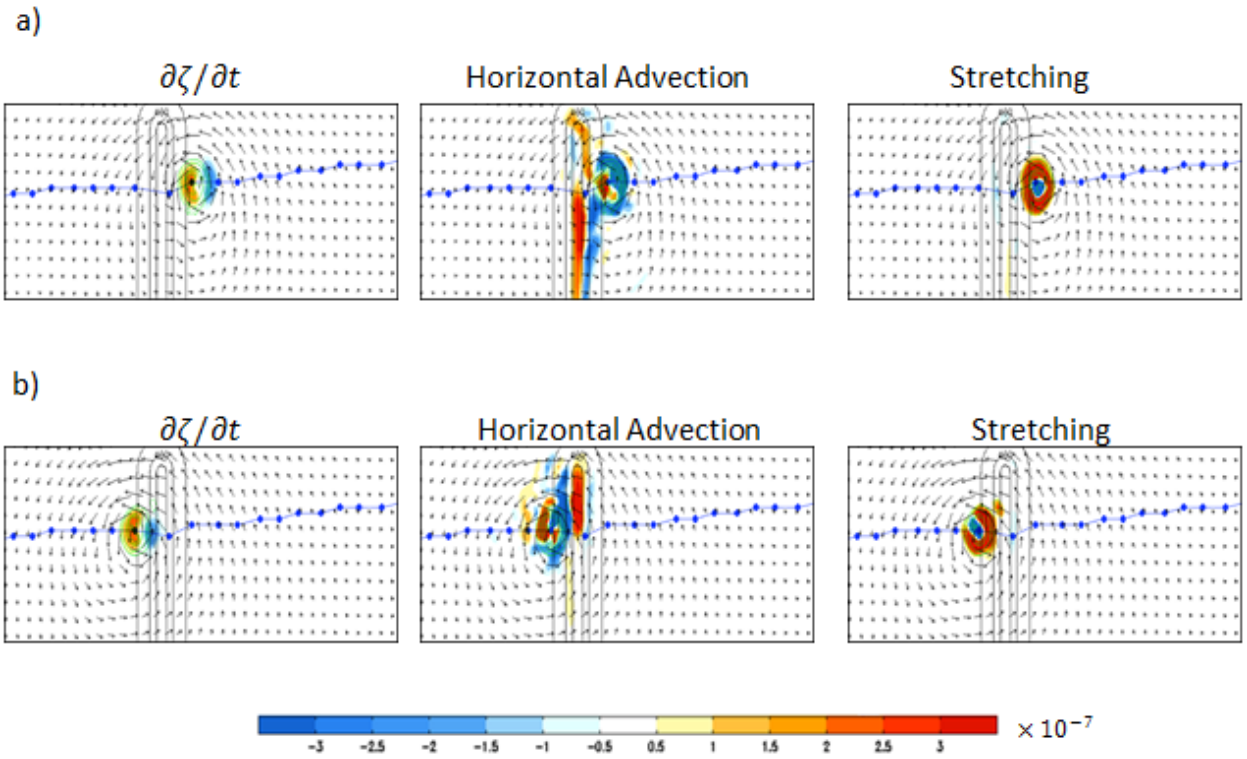

Figure 12: The vorticity budget analysis for track A1 at: a) 174 h; b) 186 h.

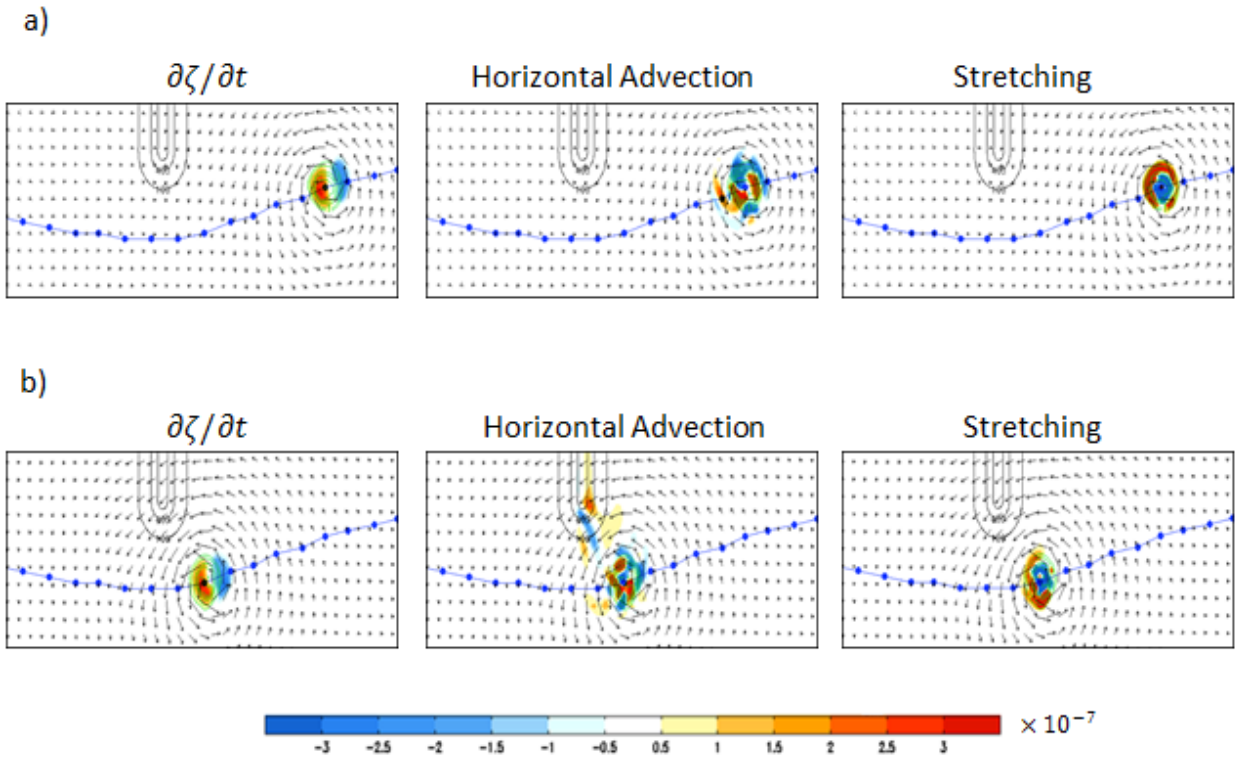

Figure 13: The vorticity budget analysis for track A3 at: a) 132 h; b) 162 h.

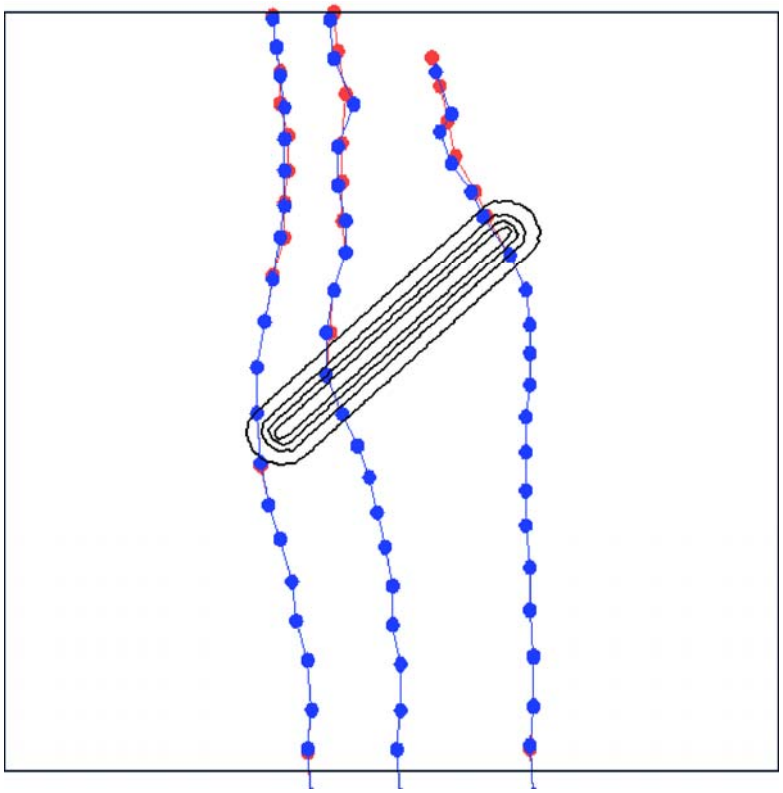

Figure 14: The TC tracks for AB1, AB2, and AB3.

a)

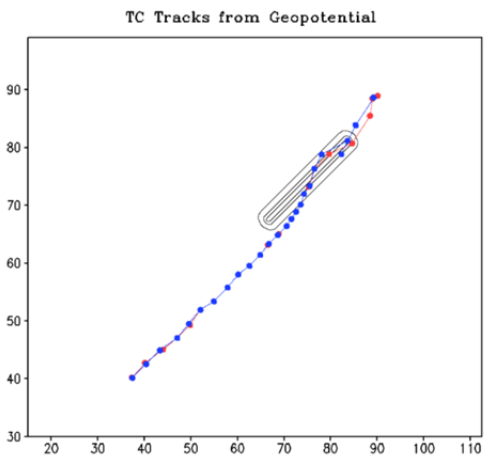

b)

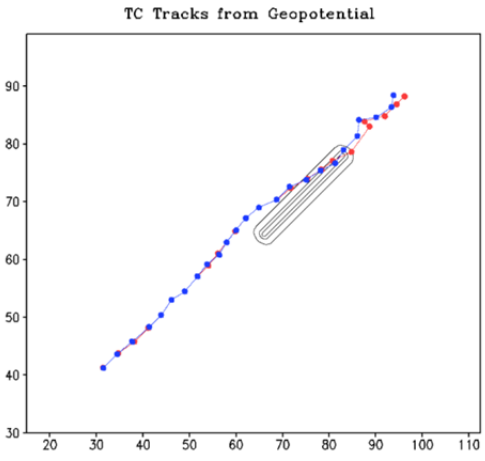

Figure 15: The TC tracks for: a) track B; b) track C.

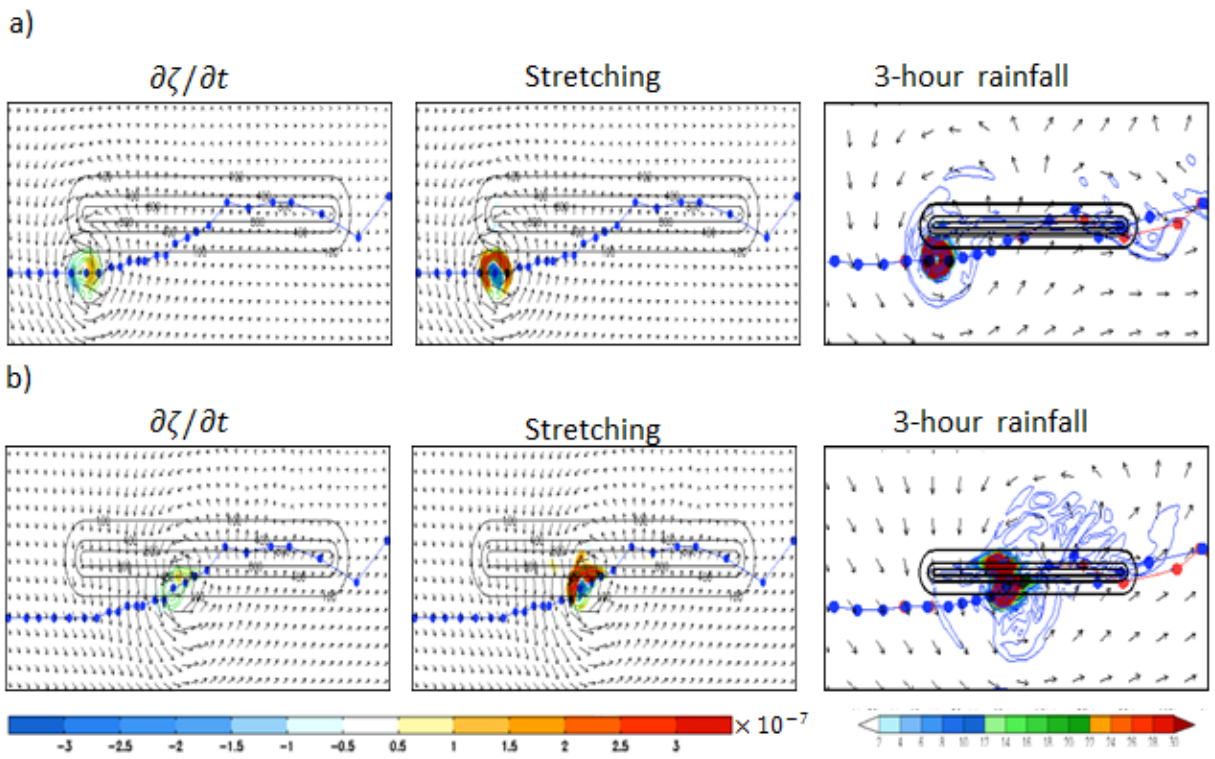

Figure 16: The vorticity budget analysis for track B at: a) 150 h; b) 204 h.

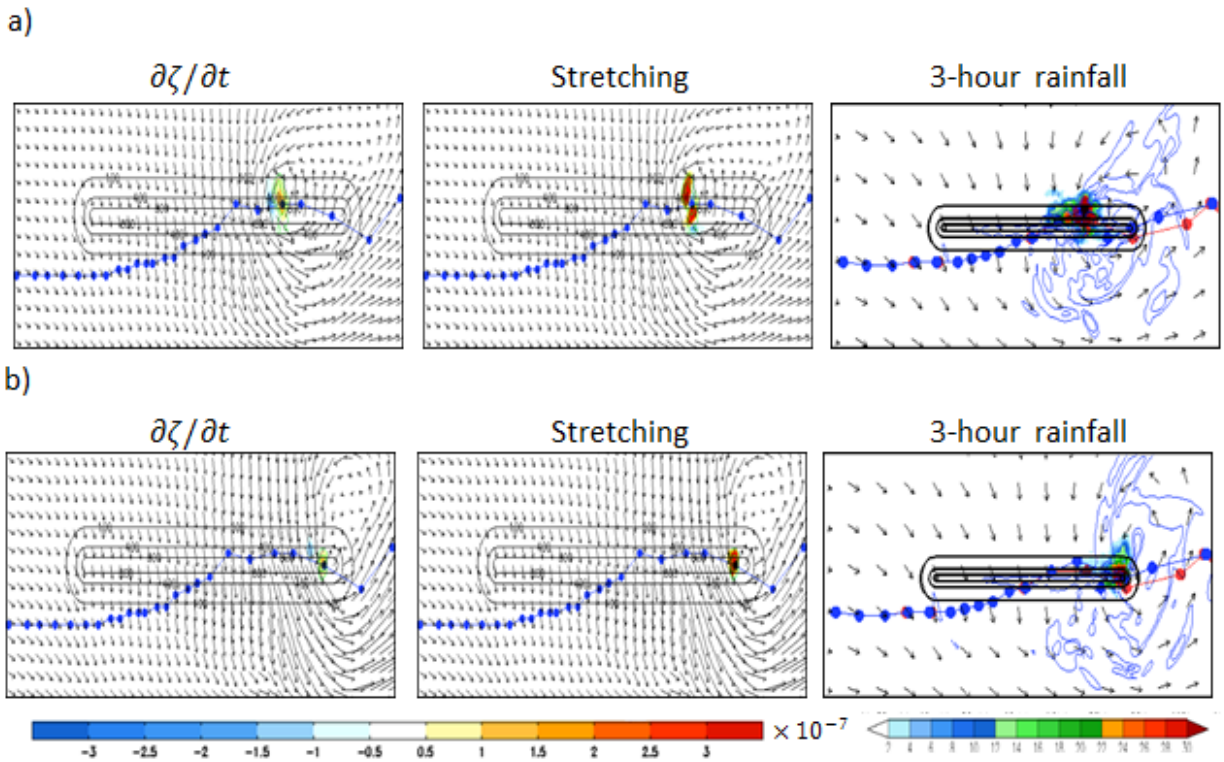

Figure 17: The vorticity budget analysis for track B at: a) 240 h; b) 252 h.